Spherical K-Means and Elbow Method Optimizations With Fisher Statistics for 3D Stochastic DFN From Virtual Outcrop Models

GRACIELA RACOLTE [1], **ADEMIR MARQUES, JR.** [1], **LEONARDO SCALCO** [1], **LEANDRO TONIETTO** [1], **DANIEL CAPELLA ZANOTTA** [1], **CAROLINE LESSIO CAZARIN** [2], **LUIZ GONZAGA, JR.** [1], **(Member, IEEE), AND MAURÍCIO ROBERTO VERONEZ** [1]

[1] Vizlab|X-Reality and Geoinformatics Laboratory, Graduate Programme in Applied Computing, Unisinos University, São Leopoldo 93022-750, Brazil
[2] CENPES-PETROBRAS, Rio de Janeiro 21941-915, Brazil

Corresponding author: Graciela Racolte (gracielarr@unisinos.br)

ABSTRACT Fracture modeling plays a valuable role to understand the fluid flow in carbonate reservoirs. For this, the fracture characterization to generate Discrete Fracture Networks (DFNs) can take advantage of analogue outcrops through Virtual Outcrop Models (VOMs), acquired by Unmanned Aerial Vehicles (UAV) and digital photogrammetry. The stochastic DFN generation is an important step in reservoir modeling as it brings more representative data to the process and has long been studied. However, optimizations concerning automatizing some of the steps necessary to its generation like data clustering are still open to advancements. In this sense, this work aims the fracture data clustering and the definition of the number of clusters when gathering data for the stochastic process, developing an Elbow method for spherical data and a balanced K-means, both based on Fisher statistics. For this, we interpreted fracture planes in a VOM that recreates a carbonate reservoir analogue from the Jandaíra Formation, in the Northeast, Brazil. As result, we show a workflow for immersive fracture interpretation alongside a 3D stochastic DFN model with fracture intensity of 22.57m^{-1} for cell sizes of 1m^3. Regarding the clustering balance, our method achieved a lower standard deviation between sets while maintaining the Fisher values greater to obtain fracture sets with lower dispersion. Additionally, the Elbow method implementation proved a beneficial step to the workflow as it reduced the interpretation bias of family clusters. These results alongside the proposed workflow bring a better understanding of the outcrop geometry while offering data scalability for reservoir modeling.

INDEX TERMS 3D stochastic DFN modeling, Elbow method, Fisher statistics distribution, K-means optimization, spherical data clustering.

I. INTRODUCTION

Carbonate reservoirs (e.g., Pre-salt of the South Atlantic Margin offshore Brazil) host important hydrocarbon reserves. The carbonates present intrinsic characteristics of porosity and permeability that regulate fluid storage and fluid flow in reservoirs [1]–[3]. These characteristics are impacted by diagenetic processes, dissolution, and tectonic events that affect the reservoirs, generating fractures and discontinuities [4]. Thus, the fracture attributes contribute to the estimation of

the geomechanical behavior of carbonate rocks necessary for hydrocarbon extraction.

Fractures can be defined as a result of a rupture or crack in the rock body that generates a physical discontinuity [5]. They often appear as a connected network of fractures, usually represented in numeric terms as Discrete Fractures Networks (DFNs) [6].

Identifying this kind of features is also an important task when analyzing impact flow on geothermal reservoirs [7], hydrocarbon-bearing formations [8], groundwater aquifers [9], leakage of CO_2 storage [10] and nuclear waste [11] broadening the knowledge over these

The associate editor coordinating the review of this manuscript and approving it for publication was Yizhang Jiang.

formations allowing proper exploration and preemptive actions.

Specifically, deep reservoirs, like Brazil's offshore pre-salt reservoirs (6km below sea level), suffer from the limitations in spatial resolution of the seismic assessment and with the sparsity of well log data [12]. These limitations in reservoir assessment lead us to the study of analogue outcrops, which are exposed rock formations with characteristics of composition and geometry similar to the reservoirs studied [13].

The fracture network investigation in analogue outcrops is carried out by direct measurements like the scanline method, where information such as length, strike and dip, and aperture are acquired [14], [15], usually by an analyst *in situ*. Due to access restrictions and limited spatial coverage, remote sensing techniques, to obtain the Virtual Outcrop models (VOMs), are widely used to obtain a larger set of geometric information about fractures on the outcrop. In this case, the interpretation of fractures can be made directly on the computer screen.

Either in situ or using VOMs, the fracture network information also integrates roughness, connectivity, and spacing, which are is modeled in deterministic and stochastic DFN models [6]. In the deterministic DFN model, attributes such as density and intensity are generally estimated by the P_{xy} system [16]. The fracture intensity is obtained by the number of fractures that cross a scan line (P_{10}), by the sum of the fracture lengths, divided by the area measure of the sample region (P_{21}), and by the sum of the areas of fractures contained in a volume (P_{32}) expressed in meters (m^{-1}). A linear correlation can be estimated observing the indexes P_{10}, P_{21}, and P_{32}, allowing the estimation of the volumetric P_{32} from 1D and 2D data [12], [17]. Such correlations are supported by a constant C, based on the parameters of fracture orientation, radius size distribution and orientation of the sampling window or scan line [18].

To estimate the P_{32} index, the dimension of the sample to be measured must be three-dimensional, in which orientation measurements (strike/dip) are performed. This information can be incorporated into the stochastic DFN modeling and scaled to the reservoir models. In these models, the quality of the simulation is directly related to the collection of information from the fracture network [17]. The orientation parameters, needed to create the DFN models, must consider their mean values and dispersion values obtained with Fisher distribution statistics [19], [20], and the quantity of sets decision will influence how the fracture are clustered and how the Fisher statistics will be propagated to the stochastic model.

Works that have generated 3D stochastic DFN models from strike/dip data relied on visual interpretation of fracture sets in diagrams and statistics generated by 2D software like the FracPaQ [21], [22] and FRACMAN [23] to identify the best quantity of sets. With some works [24], [25] reducing the number of sets arbitrarily applying metrics to identify and agglutinate co-planar sets, also using the Fisher concentration to highlight the possible number of clusters in the stereonet. Additionally, some works have proposed modifications to

the clusterization method based on the K-means algorithm, employing Particle Swarm Optimization and Fuzzy clustering [25], [26], also optimizing the clusters initial positions. However, the quantity of cluster is still set arbitrarily.

In this regard, we propose two optimizations to the 3D stochastic DFN generation workflow by: adapting the Elbow method to the definition of fracture sets using the spherical K-means and Fisher statistics; and making a balance check to the clusters obtained from the K-means algorithm to verify if the process should be restarted with new center positions or not. These strategies aim to obtain better input data to the Fisher statistics definitions necessary for the stochastic generation modeling.

For this, we use the software Mosis XP [27], [28], to interpret fracture planes in a VOM obtained of an outcrop analogue located in the Jandaíra Formation, in the Brazilian Northeast. From this data, our proposed workflow is applied and validated by generating a 3D stochastic DFN and estimating the volumetric fracture intensity for the model cells. This region is well studied in geological terms [29], [30], however no study regarding outcrop geometry and generation of 3D stochastic was carried. This work is presented as follows: the proposed method, statistics, and computations to extract 3D data are presented in Section 2; the interpretation scenario and experimental setting are presented in Section 3; followed by the results and comparisons in Section 4; accompanied by the discussion and conclusion.

II. 3D STOCHASTIC DFN MODELING

The proposed workflow to determine the volumetric intensity integrates the 3D stochastic DFN generation from VOM interpretation of fracture planes, as illustrated in Figure 1.

The workflow starts with the fracture plane points acquisition from VOM. The rest of the workflow describes the data clustering and statistics for each possible set, and finishes with the 3D fracture generation and the volumetric 3D DFN. This workflow is better described in the following sections.

A. PROCESSING FRACTURE PLANE DATA

The interpreted plane data extracted from the VOM is composed of 3D point coordinates (*xyz*), in which the positional and directional information will be computed. Directional and positional information from points placed in 3D space necessary for fracture characterization can be obtained by basic geometry operations. As the first plane information, the centroid is calculated to obtain the central position of a group of points, given by

$$centroid = \frac{\sum_{N}^{i=1} x_i}{N}, \frac{\sum_{N}^{i=1} y_i}{N}, \frac{\sum_{N}^{i=1} z_i}{N} \quad (1)$$

where N is the quantity of points that compose the plane and $x_i \in \{x_0, x_1, \ldots x_N\}$, $y_i \in \{x_0, y_1, \ldots y_N\}$, and $z_i \in \{z_0, z_1, \ldots z_N\}$ are the points coordinates.

The next plane information is the plane equation and its components that are given by
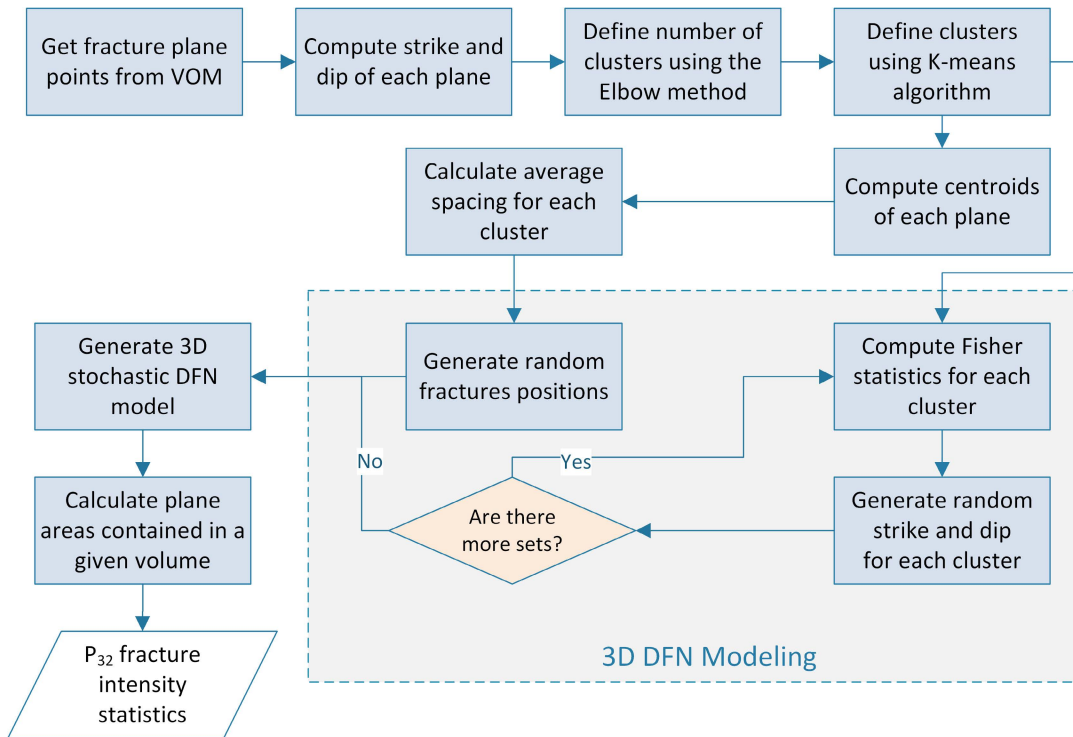
$$Ax + By + Cz + D = 0 \quad (2)$$

FIGURE 1. Proposed workflow for 3D stochastic DFN generation and fracture intensity estimation P_{32} from fracture planes measured in VOM.

where A, B, C, and D are the equation terms (with D representing a positional term) [25]. These terms are computed with the principal component analysis (PCA) technique [31] that fits the point data to its eigenvalues and eigenvectors, where the third eigenvector gives the plane normal vector $N(A, B, C)$ usually normalized in the form $n(a, b, c)$. The positional term D in the plane equation is given by

$$D = centroid \cdot n(a, b, c). \quad (3)$$

After obtaining the plane equation terms, the strike and dip angle are calculated in terms of α and β angles given by

$$\alpha = arccos\left|\frac{c}{\sqrt{a^2 + b^2 + c^2}}\right| \quad (4)$$

and

$$\beta = q \pm arccos\left(\frac{a}{\sqrt{a^2 + b^2}}\right) \quad (5)$$

where q é $0°$, $180°$ or $360°$ according to the quadrant that the resultant vector of a and b points [32].

These equations give us the strike and dip in radians, which are later converted to degrees for visualization in the stereonet and other statistics. Depending on the quadrant, we must correct the strike direction considering the a and b values, where, if a and b are greater than zero the strike is $360 - deg(\beta)$ and if a is greater than zero and b is lesser than zero the strike is $180 + deg(\beta)$. Also, considering the "right-hand rule" [33] we consider opposite strike directions as the same angle, computing directions for the first and the second quadrant only.

B. FISHER STATISTICS

The strike and dip data obtained from the 3D interpretations are the main data for the stochastic plane generation. However, this data is reduced to spherical statistics information computed with Von Mises and Fisher [34] statistics for each fracture set. The Fisher statistics [35] are spherical statistics that indicate the dispersion and distribution of point positions in a sphere. For the Fisher statistics, the mean strike and dip for a set are observed in terms of the normal vector of each plane represented in polar coordinates ϕ and θ. Where ϕ (latitude) is given by $90 - dip$, and θ (longitude) is given by the angle rotated from the prime meridian using the bearing angle.

The mean direction of Fisher is given by the sum of the direction cosines [35]

$$\bar{l} = \sum_{i=1}^{N} l_i \quad \bar{m} = \sum_{i=1}^{N} m_i \quad \bar{n} = \sum_{i=1}^{N} n_i \quad (6)$$

where $l_i = cos(\phi_i)cos(\theta_i)$, $m_i = cos(\phi_i)sin(\theta_i)$, $n_i = sin(\phi_i)$, and i is an individual plane of the N observations.

After computing the mean direction cosines, they are converted in unit vectors dividing by the length of the dip mean vector R given by

$$R = \sqrt{(\bar{l})^2 + (\bar{m})^2 + (\bar{n})^2} \quad (7)$$

and the unit vectors are given by

$$\hat{l} = \frac{\bar{l}}{R} \quad \hat{m} = \frac{\bar{m}}{R} \quad \hat{n} = \frac{\bar{n}}{R}. \quad (8)$$

The mean directional unit vectors are converted to mean strike and dip are then given by

$$\delta = arcsin(\hat{n}) \tag{9}$$

for dip angle, and

$$strike = \begin{cases} \left[arcos\left(\frac{\hat{l}}{cos(\delta)} \right) \right] & \text{if } \hat{m} \geq 0 \\ 360 - \left[arcos\left(\frac{\hat{l}}{cos(\delta)} \right) \right] & \text{otherwise.} \end{cases} \tag{10}$$

The index of dispersion of the Fisher distribution k is given by

$$k = (N - 1)/(N - R) \tag{11}$$

where k values close to 0 indicate not coplanar planes and positive values to ∞ indicate strongly coplanar planes. In terms of distribution, the Fisher statistic [36] is given by

$$f(\phi, \theta) = \frac{k}{4\pi \sinh(k)} exp^{k[cos(\theta_0)cos(\theta)+sin(\theta_0)cos(\phi-\phi_0)]}. \tag{12}$$

C. SPHERICAL DATA CLUSTERING

The basic K-means algorithm clusters objects in sets of K defined clusters, with random centroid clusters initially set in the first iteration. The objects are then associated with the closest cluster center given a distance metric. After each iteration, the centroid position of the cluster is recalculated. The algorithm converges when no significant change in centroid positions is observed.

To obtain the optimal number of clusters for the K-means clustering the most common algorithms used are the Elbow method and the Silhouette method [37]. For the Elbow method algorithm, the optimal number of sets is given by the Elbow method in which a set of different numbers of clusters are tested evaluating the squared sum of distances of samples and clusters centers. Using a line plot as a reference, the desired number of clusters is identified by the inflection point in the graph. Our implementations modify the K-means and the Elbow method to use the Fisher k statistics to obtain optimized cluster sets.

For the K-means algorithm, we consider the spherical K-means which uses the angular distance between two strike/dip positions as polar coordinates (ϕ/θ) to measure the clusters and centers' proximity. We use an additional step that verifies if the generated clusters have optimal Fisher k values, considering that there is no set with Fisher k values below the average Fisher k minus the standard deviation of all sets. This approach guarantees that we have balanced clusters (Figure 2b), instead of some clusters with low dispersion and others with high dispersion (Figure 2a). If this condition is not met, the K-means algorithm is restarted with new random centers. These steps are detailed in Algorithm 1.

For the Elbow method algorithm, we consider the normalized squared mean of Fisher k values of all sets evaluated

(a) Original clustering method. (b) Proposed balancing method.
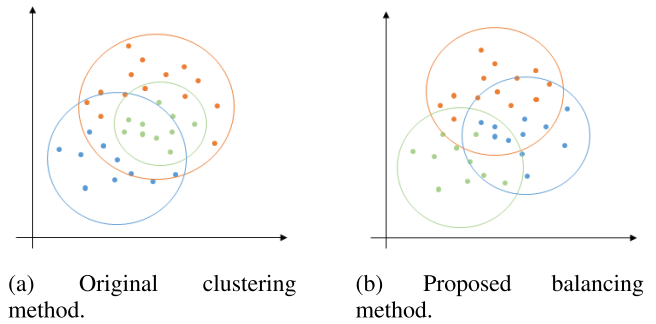
FIGURE 2. Balancing clusters effect on group dispersion indicated by each group outer circle. In a) the groups' dispersion have uneven sizes which will in our example generate a lower value of Fisher k; while in b) the groups are evenly distributed and present similar dispersion.

in each K-means K value evaluated. After running all different K-means K values clustering and after obtaining the established Elbow metric values, an additional step is carried out to compute the optimal number of clusters systematically, establishing a line between the first and last values obtained in the Elbow method. This line is used a reference to compute the most distant point from this line, as the graph inflection point. These steps are detailed in Algorithm 2.

D. SPACING

After estimating the sets and directional statistics the spacing estimation can be carried [38], [39]. The spacing, assuming that two planes are parallel, e.g. have equal values for the a, b, and c, is given by

$$SP_{12} = \frac{|d_1 - d_2|}{\sqrt{a^2 + b^2 + c^2}} \tag{13}$$

where d_1 and d_2 are two parallel discontinuities (planes). For non-parallel planes, a virtual scanline can be used to estimate the distance between planes that cross the designated line, where the average, minimum and maximum spacing can be computed [40].

E. 3D FRACTURE GENERATION AND STOCHASTIC DFN MODELING

With Fisher statistic parameters and spacing for each set, we can generate the stochastic DFN by estimating random planes that tend to follow the same Fisher distribution of the original sets when applying stochastic techniques.

This process starts by establishing the number of fracture planes to be generated for each fracture set. Our implementation considers the mean plane sizes to determine the number of fracture layers to be generated, as the height (z-axis) of the model is divided by the mean fracture size.

In each layer, the quantity (n) of fracture planes to be generated in each set is given by the width (x-axis) times the depth (y-axis) of the model divided by the set spacing.

After getting the quantity of fractures for each layer (n), we generate two lists of random uniform values R_1 and R_2 of size n. To generate the new fracture data we apply these

Algorithm 1 Spherical K-Means With Fisher k Groups Check

1: Convert Strike/dip data to lat/lon
2: **while** *optimal_Fisher_k* $\neq$ *True* **do**
3:     Get random K lat/lon positions as initial set centers
4:     **while** *moving_centers* $\neq$ *False* **do**
5:         Compute distances between centers and measures
6:         Associate measures to closest centers
7:         Change center positions to new centers position in each group
8:         **if** *distance*(*centers*, *new_centers*) $\leq$ *tolerance* **then**
9:             *moving_centers* $\leftarrow$ *False*
10:        **else**
11:            *centers* $\leftarrow$ *new_centers*
12:        **end if**
13:    **end while**
14:    Compute Fisher_k_values for each group
15:    **if** *Fisher_k_values* $\leq$ (*max*(*Fisher_k*) $* 0.25$) **then**
16:        *optimal_Fisher_k* $\leftarrow$ *False*
17:    **else**
18:        *optimal_Fisher_k* $\leftarrow$ *True*
19:    **end if**
20: **end while**
21: **Output:** *centers*

Algorithm 2 Elbow Method for Spherical Data Clustering

1: **Input:**   strike_data,   dip_data,   max_clusters, max_iterations
2: initialize *mean_fisher_k* array
         ▷ Compute *mean_fisher_k* for *max_iterations* runs for clusters from 1 to *max_clusters*
3: **for**   *i_cluster*   =   1, *i_cluster*   < *max_clusters*, *i_cluster*++ **do**
4:     sum_fisher_k = 0
5:     **for** $i = 1, i <= max\_iterations, i++$ **do**
6:         Get clusters and clusters centers from spherical kmeans;
7:         Compute Fisher statistics K;
8:         *sum_fisher_k* = *sum_fisher_k* + *K*;
9:     **end for**
10:    *mean_fisher_k*[*i_cluster*]   = (*sum_fisher_k*/*max_iterations*)^2;
11: **end for**
                            ▷ Triangulate the squared *mean_fisher_k* as positions in a graph and get the point with longest distance to the reference line
12: $x1, x2 \leftarrow$ first and last values from *mean_fisher_k*
13: $y1, y2 \leftarrow$ first and last index positions from *mean_fisher_k*
14: Initiate *distances* array
15: **for** $i = 1, i < max\_clusters, i++$ **do**
16:    $x_i = i$
17:    $y_i = mean\_fisher\_k[i]$
18:    *numerator* $\leftarrow abs((y2 - y1) \times x_i - (x2 - x1) * y_i + x2 \times y1 - y2 \times x1)$
19:    *denominator* $\leftarrow \sqrt{(y2 - y1)^2 + (x2 - x1)^2}$
20:    *distances*[*i*] $\leftarrow$ *numerator*/*denominator*
21: **end for**
22: *ideal_n_clusters* $\leftarrow$ position of the highest value on *distances*
23: **Output:** *ideal_n_clusters*

random values in the Fisher distribution sampling function given by

$$\theta = 2 \arcsin \sqrt{-log[R_1(1 - \lambda) + \lambda]/2k} \quad (14)$$

and

$$\phi = 2\pi R_2 \quad (15)$$

where k is the Fisher dispersion, and $\lambda = exp(-2k)$. Which are rotated using the rotation matrix given a initial θ_0 and ϕ_0. The rotation matrix used to obtain the final sample values θ' and ϕ' is given by

$$A(\theta_0, \phi_0, 0) = \begin{pmatrix} \cos\theta_0 \cos\phi_0 & \cos\theta_0 \sin\phi_0 & -\sin\theta_0 \\ -\sin\phi_0 & \cos\phi_0 & 0 \\ \sin\theta_0 \cos\phi_0 & \sin\theta_0 \sin\phi_0 & \cos\theta_0 \end{pmatrix}$$
$$(16)$$

The random generated plane directions are then converted to their normal vector information to be placed in the stochastic DFN following uniform random positions for each layer.

To estimate the volumetric fracture intensity P_{32} we consider a sample volume with the same size and position as the stochastic DFN model, while this volume is subdivided into cells of equal sizes. In each cell, we compute the fracture plane intersections with the cell faces to obtain the vertices that make the fracture portion polygon inside the cell to compute its area.

These intersections are obtained using the Möller-Trumbore ray-triangle intersection algorithm [41] considering the cell faces and fracture planes as triangle pairs and the rays as triangle vertices. Fracture plane vertices inside the cells are identified using the Delaunay triangulation using the cell edges as reference.

The polygon areas using the extracted vertices are computed by subdividing the polygon using the Delaunay triangulation and estimating the area of triangles that fit the polygon. All polygon areas inside a sample cell are summed and then divided by the volume to compute P_{32} for each cell.

The generated algorithm and scripts presented are packaged in an application named vizfrac3D which will generate the following products as presented in Figure 3. This chart illustrates what a user could expect in terms of input and output to our script in an easier way, complementing the main workflow presented in Figure 1.

III. METHOD VALIDATION
A. STUDY AREA AND GEOLOGICAL SETTINGS
For this study we used a ravine within the Lajedo Soledade (Figure 4B), located in Apodi municipality,
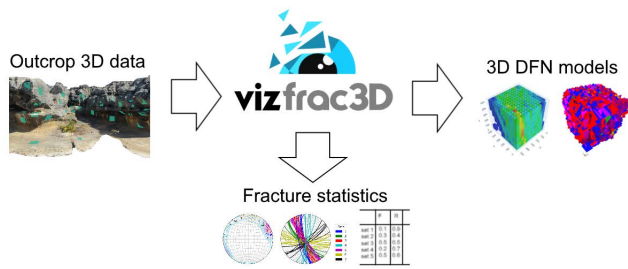
FIGURE 3. Application for 3D stochastic DFN generation vizfrac3D.

in the Rio Grande do Norte state, Brazil. This outcrop presents rocks within the southeast portion of the Potiguar Basin [42], [43], precisely within the Jandaíra formation (Figure 4A), deposited between Turonian and Campanian stages (*ca.* 93.9-83.6 Ma) [29], [44].

This formation is characterized by the presence of a monotonous and homogeneous succession of carbonate rocks predominantly classified as mudstones, grainstones, and packstones, composed of grains of primary carbonate minerals (calcite) with the strong posterior transformation of primary minerals for dolomite [30], [46], [47]. Grainstones are grain-supported rocks and have a relatively small fraction ($<1\%$) of clay-like grain material ($<20\mu m$), while packstone is a supported rock by grains, but with a clay fraction ratio $>1\%$, and mudstones are not supported by grains and are predominantly formed by fragments of grain size $<20\mu m$ [48]. The rocks have a minority fossiliferous content of bivalves, mollusks, and algae remain [46].

The Jandaíra Formation is locally preserved in an expansion that exceeds 600m in thickness with a slight bedding dip (< 5 degrees) to NNE at the regional level [47], [49]. This late Cretaceous formation comprises a fracture network that is predominantly in the N-S; E-W directions, and secondarily NE-SW and NW-SE directions [44], [47], in both cases with sub-vertical dips associated to the tectonic evolution of the Potiguar Basin. This fractured system is characterized by vertical or sub-vertical joints and veins. Horizontal fractures and fracture parallel to the Jandaira formation bedding also occur. These structures are possibly related to the lithostatic pressure relief process in the Potiguar Basin region [44], [50].

The presence of calcite veins with N-S, NNE-SSW, and E-W directions are reported by [50], while stylolites oriented predominantly in E-W and NNW-SSE directions are found by [47]. Additionally, there is formation of circular to sub-circular subsidence structures, such as sinkholes and rebate rings, given by the dissolution and patent structuring of the Jandaíra Formation, which sustains high plateaus of regional character with main directions NE-SW [44], [47], [50].

Given the geological characterization and the extensive areas of naturally fractured carbonate outcrops present in the Jandaíra Formation, this region is of great interest for geological studies focused on hydrocarbon reservoirs, like the pre-salt reservoirs, in the Brazilian offshore. The Lajedo

Soledade outcrop, in particular, has NE-SW faults and E-W fractures, which control its drainage system [29]. This outcrop presents an important process of karstification resulting from the dissolution of carbonate rocks by meteoric waters, as described in [29], which led to the creation of cavities such as the ravine used for this study. The karst dissolution process in the ravine, as well as the characterization of stylolites and primary discontinuities are best described in [30], based on field and laboratory analyses. However, a more comprehensible geometric analysis of these features is yet to be seen, and this is one key motivation for this work.

B. VOM ACQUISITION

For the UAV image acquisition in the ravine, we used a DJI Mavic 2 Pro embedded with a Hasselblad 20 Megapixels camera. The ravine represents 7,000m² of the outcrop, in which 376 photos were taken with a camera tilt of 45°, in a flight lasting 14 minutes and height of 3m for subsequent photogrammetric reconstruction and generation of the textured 3D model.

The photogrammetric reconstruction follows the flow (Figure 5) proposed by the software Agisoft Metashape®[1] - version 1.6.2, which employs algorithms of SfM [51], [52] identifying key points (Scale-invariant Feature Transform - SIFT algorithm) in image pairs, and through bundle adjustment estimate camera location to generate the point cloud, whereafter the Multi-View Stereo algorithm [53], [54] is used to create the dense point cloud. The dense point cloud is triangulated generating a 3D mesh that will be texturized generating the VOM.

C. FRACTURE INTERPRETATION IN IMMERSIVE ENVIRONMENT

We used the software Mosis XP designed for geological interpretation in an immersive virtual reality (iVR) system with a head-mounted display (HMD) to extract the fracture planes. This software integrates the Mosis[2] suite, developed by the Vizlab | X-Reality and GeoInformatics Lab.[3] With the iVR system set, the VOM is loaded on Mosis XP project ready for immersive geological interpretation where in this work we use 3D data from the plane measurement tool exported as *xyz* data.

The HMD used is an HTC Vive with a pair of controllers (also visible within the software) tracked by two infrared towers. The computer specs required for the iVR system are relatively high due to the dual visual output of the HMD (one for each eye) at a high refresh rate (90Hz) to avoid motion sickness. The computer setup is an Intel Core i7-6820HK 2.70GHz (3.60GHz) CPU, 64GB RAM, an Nvidia GTX 1080 8GB RAM graphic card, and Windows 10, 64-bit operational system.

---

[1] http://www.agisoft.com/downloads/user-manuals/

[2] mosis.vizlab.cc
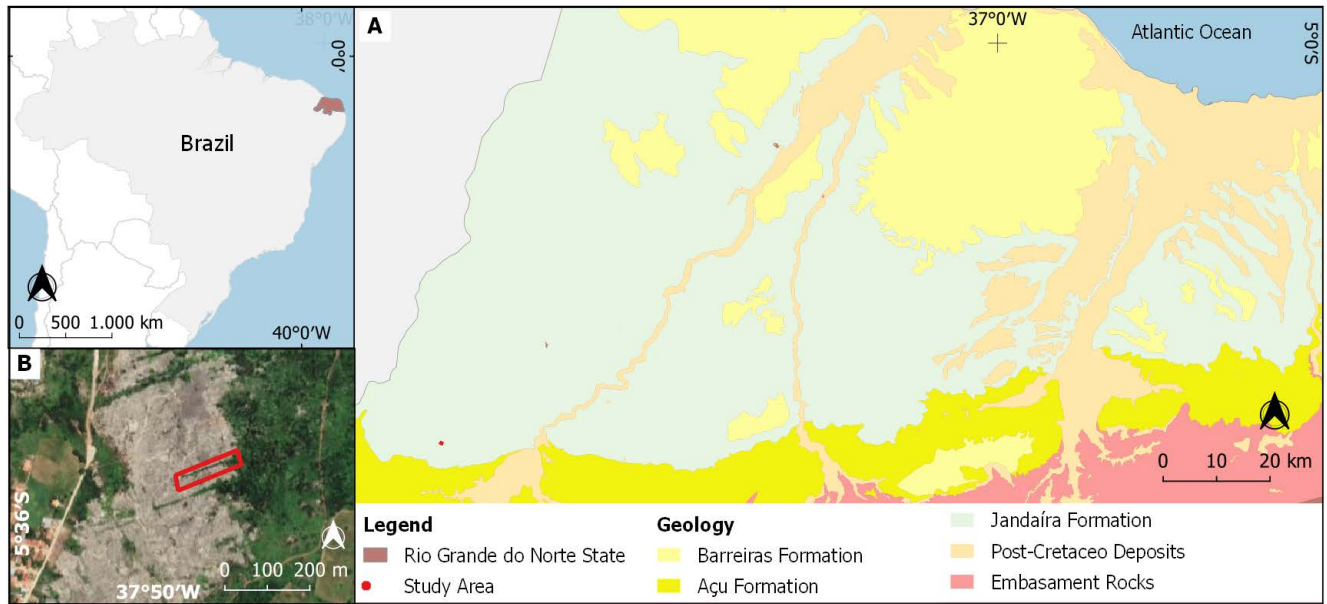
[3] http://www.vizlab.unisinos.br/

FIGURE 4. Study area location: A - Geological Formations belonging to the Potiguar Basin, in the Rio Grande do Norte state, Brazil, adapted from [45]; B - Lajedo Soledade outcrop, with the ravine delimited in red. Reference System: World Geodetic System 1984 (WGS84).
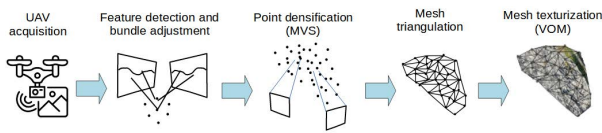

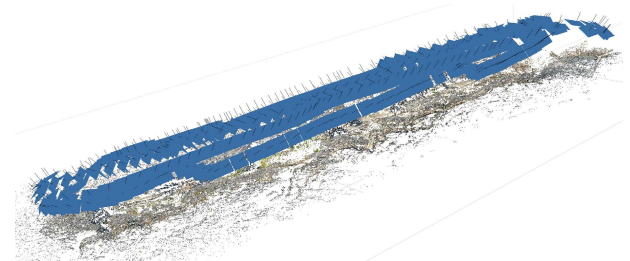**FIGURE 5.** Common SfM/MVS workflow to generate 3D texturized models from UAV image acquisition.

D. VALIDATION

For validation of the proposed method to generate the 3D stochastic DFN, we evaluate the Fisher statistics of both stochastic and deterministic models. Each generated and interpreted set will have a mean strike and dip, that considering the polar coordinates, is possible to determine the angular distance between the stochastic and deterministic fracture sets. This validation is done considering 30 stochastic generations for each fracture set where we compute the mean and standard deviation of the angle distance.

To validate the proposed method to balance the K-means clusters after the elbow method definition, we run the original spherical K-means clustering and the modified proposed method 10 times for each set considering a small subset. The dispersion Fisher k value is used in terms of mean, standard deviation, min and max values to show the impact of the proposed method.

E. EXPERIMENTAL SETTINGS

The fracture plane data from Mosis XP consists of x,y, and z coordinates which are converted to strike, dip, and centroid data following the steps presented in the prior section, while the algorithm to obtain the optimal number of clusters or fracture families is presented in Algorithm 1. We use the average of 50 runs as max iterations considering 1 to 10 clusters.

FIGURE 6. Point cloud generated from photo alignment in the Agisoft Metashape software.

After computing Fisher and spacing statistics the fracture planes for the 3D DFN model are generated. The volumetric sampling, in this case, will give the P_{32} areal fracture intensity per volume with mean and standard values.

The 3D stochastic model to be generated will have a size of $20m^3$ with individual cube samples of $1m^3$, while fracture planes will have $4m^2$.

IV. RESULTS

The UAV-SfM-MVS photogrammetric processing (Figure 6) resulted in a textured 3D model with 899,055 triangles faces and texture resolution of 6 times 8k pixels showed in Figure 7a. The iVR interpretation is illustrated in Figure 7b, where we captured 638 planes using the bedding plane tool (Figure 7c). Lastly, the measured plane locations are shown in Figure 7d.

Applying the Elbow method in the fracture plane data from the iVR interpretation, we identified the optimal number of clusters as shown in Figure 8, highlighted by the inflection point with 7 clusters.
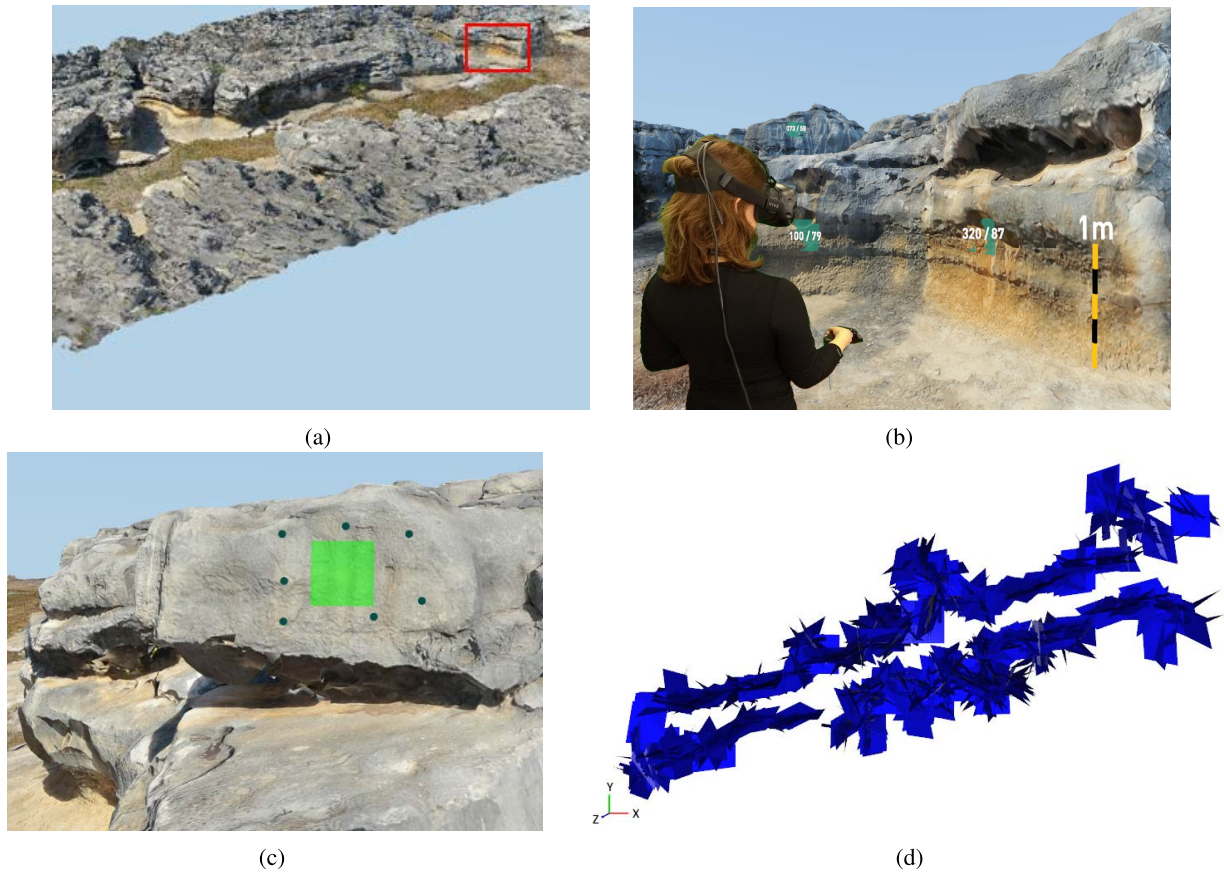
FIGURE 7. Fracture interpretation in Mosis XP in immersive mode. The red marked area in (a) is detailed in (b) showing the measured planes and scale. In (c) the points marked to capture fracture planes and in (d), illustration of the planes captured in the outcrop.

TABLE 1. Result validation for the proposed clustering balancing considering Fisher k values not lower than 25% range of the max value against the unmodified random spherical K-means considering 10 runs (70 random groups for each method).

Fisher k-values	μ	σ	min	max
Original	94.15	79.74	1.02	496.07
Balanced	78.90	31.36	30.43	151.20
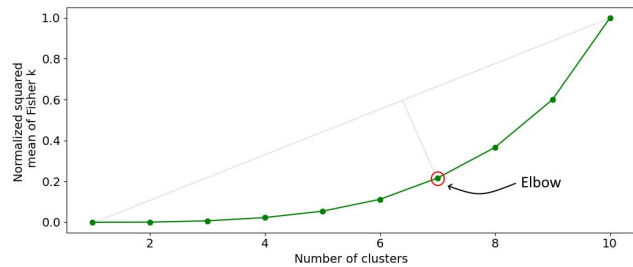
FIGURE 8. Elbow method with 10 different cluster sizes.

FIGURE 9. Stereonet with fracture poles clustered using the proposed method considering 7 clusters identified by the Elbow method.

method achieved Fisher k values closer to 1 indicating groups with no directional trend.

Within each of the seven clusters shown in Figure 9 we computed the Fisher statistics as shown in Table 2, while a visual representation of the Fisher dispersion is shown in Figure 10.

The mean (μ) and standard deviation (σ) of the spacing in each set were also calculated as shown in Table 3. Set families with high mean and standard deviation spacing are guaranteed to have at least one fracture represented in the final model.

In Figure 11 the stochastic model is shown with the fracture generated for each set, alongside the volumetric model with 8,000 sample blocks colored according to the volumetric fracture intensity P_{32}, which presented a mean intensity of $22.57\mathrm{m}^{-1}$, and standard deviation of 7.92.
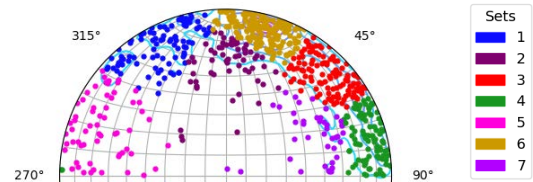
Table 1 shows the results of the clustering balancing method in comparison to the original spherical clustering, where in 10 runs for each of the selected number of clusters considering a subset of 10% of the data, the proposed method showed a lower standard deviation (σ). Also, the unmodified
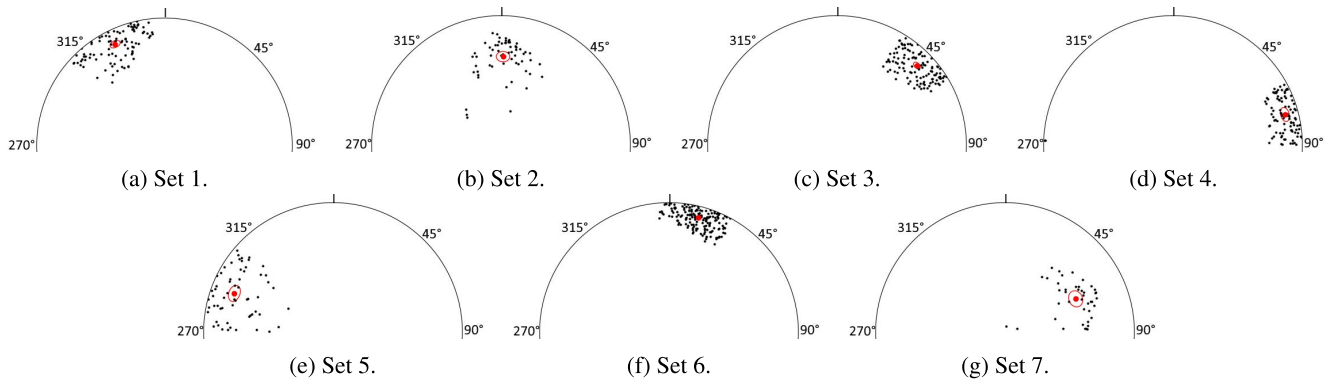
FIGURE 10. Visual representation of the Fisher dispersion for each set is shown as the red circle radius.
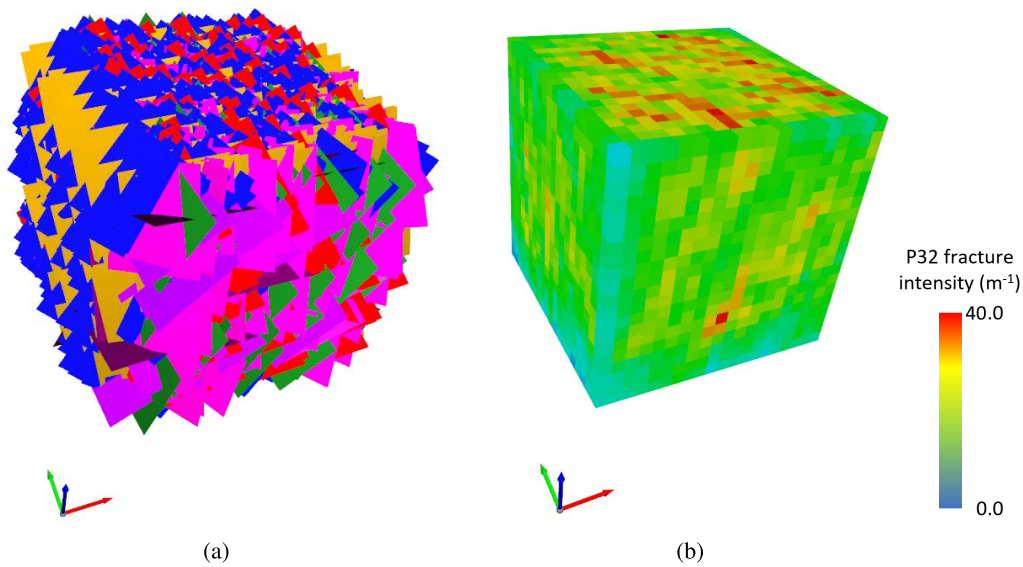

FIGURE 11. Stochastic generated fracture model considering the Fisher statistics and spacing for each set in (a), and volumetric fracture intensity model (b) with individual sampling volume of 1m³, with 20m³ total in both models.

TABLE 2. Directional statistics for each set showing mean direction/mean dip and computed dispersion values and Fisher angles.

Set	Mean Strike/Dip	Fisher Angle	R-Value	k-Value
1	64°/77°	2.69°	0.97	31.08
2	91°/58°	3.70°	0.96	24.38
3	135°/76°	2.00°	0.98	44.53
4	165°/79°	3.49°	0.94	17.55
5	21°/71°	4.25°	0.95	19.27
6	104°/80°	1.42°	0.98	59.80
7	155°/51°	4.70°	0.96	23.00

TABLE 3. Spacing information regarding fracture planes for each set. *n* indicates the number of planes contained in each set.

	Set 1	Set 2	Set 3	Set 4	Set 5	Set 6	Set 7
n	92	63	114	99	61	167	42
μ	1.47	21.34	4.78	7.55	3.85	2.31	14.27
σ	1.61	30.40	7.78	14.68	5.03	3.75	19.58

The Figure 12 shows the stereonets with fracture planes generated for each clusters, matching the Figure 10, while the number of fracture planes generated are shown in Table 4.

TABLE 4. Quantity of fracture planes generates for each set.

	Set 1	Set 2	Set 3	Set 4	Set 5	Set 6	Set 7
n	1360	90	415	260	520	860	140

For the stochastic process validation considering 30 stochastic runs, we achieve low deviation on the distance angle values indicating the statistical stability, while the mean angle distances are minimal indicating that the stochastic generations replicated the same behavior found in the deterministic model as shown in Table 5.

V. DISCUSSION

The first of the proposed improvements, namely the modified Elbow method to identify the optimal number of clusters (Figure 8), proved an important step in the stochastic DFN generation workflow as it reduces the bias when selecting the number of fracture sets from the gathered data. It also contributed to generating fracture data respecting a lower
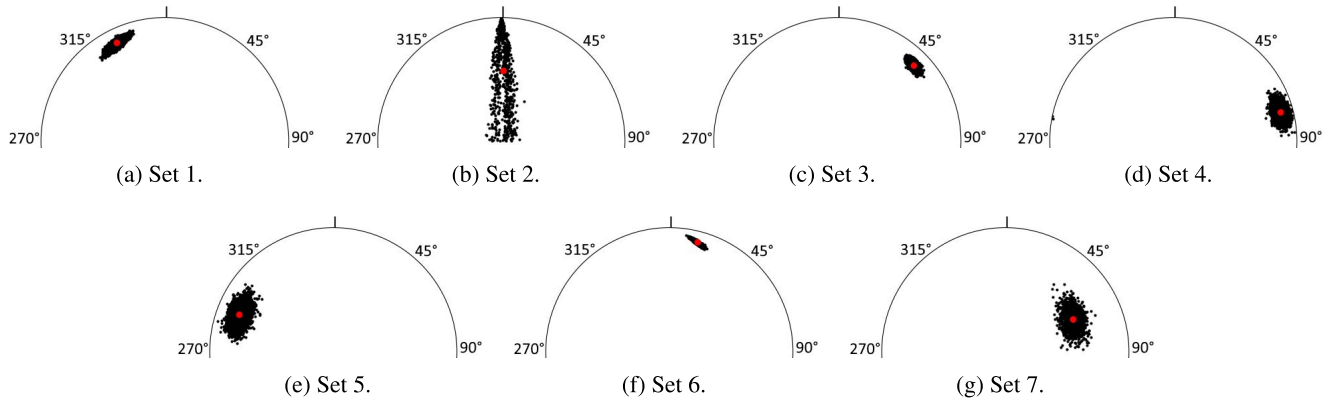
FIGURE 12. Visual representation of the Fisher dispersion for each stochastic set is shown as the red circle radius.

TABLE 5. Deterministic and stochastic mean strike/dip from each set and mean angular distance computed for method validation considering 30 stochastic generations.

Set	Deterministic	Stochastic (Mean)	μ distances	σ distances
1	64°/77°	64°/77°	0.0012°	0.0008
2	91°/58°	92°/47°	0.1914°	0.0518
3	135°/76°	135°/76°	0.0017°	0.0010
4	165°/79°	165°/79°	0.0049°	0.0026
5	21°/71°	22°/71°	0.0056°	0.0024
6	104°/80°	104°/80°	0.0011°	0.0007
7	155°/51°	155°/51°	0.0016°	0.0055

direction dispersion used for the Fisher generation. This is a crucial factor as a reduced number of sets can generate sets that do not follow a visible trend, and prior works like [21]–[25] have generally ignored these characteristics of groups' dispersion.

Additionally, the proposed clustering balancing using the Fisher *k* values of dispersion guarantees that the selected clusters will follow a more defined trend. This is shown in our validation step as without our method, the K-means spherical clustering generated groups with values as low as 1.02 for the Fisher *k* value of dispersion, while the balanced results presented a minimum value of 30.43 and a lower standard deviation between groups (Table 1). Our approach tackle a concern also find by [25], [26], however, they only adjust the ideal position of clusters centers and not the final clusters.

With cluster balancing, the data distributed in the sphere in their respective sets shown in Figure 9 and the results presented in Table 2, prove the validity of the proposed method. Additionally, from the proposed optimizations, our stochastic model is able to reproduce the input data (10 and 11) with average strike/dip differences equal to 0.03°, having a set with a difference of 0.19° and all others with values less 0.006° (Table 5).

Regarding the DFN modeling, an important aspect to be set is the plane form and dimensions that represent the fracture, while the most common forms are ellipsoidal, rectangular, or with the planes extending to infinity. This will impact how the area of the plane will be measured to estimate the

fracture intensity in the volume P_{32} or how the topology will be constructed as suggested by [55]. However, the squared shape represented was the most appropriate to our fracture model. Besides that, the sample volume size needs to be further explored, as prior works have employed sizes varying from centimeters to tens of meters [21], [56]–[58].

As for the VOM interpretation, the constant evolution and improvement of UAV-SfM-MVS techniques for generating VOMs have resulted in increasingly lighter meshes [59], which can increase the accessibility for such immersive interpretations, as performance capabilities of today's computers, graphic cards, and HMDs enable more people to experience virtual reality.

The studied area presents steep and narrow sinkholes and canyons from karstification and subsequent erosion of these faults [29], [30], which makes access to these places difficult and dangerous. The adequate collection of fracture planes was possible due to the particularity of the immersive virtual environment that allows navigating the outcrop safely and reaching places that would not be possible in a real environment. Thus, the proposed framework showed a viable alternative as a mean to safely provide three-dimensional fracture data in adequate quantity and quality for the generation of numerical models from realistic fracture networks, which reinforces previous work on these themes [60], [61].

VI. CONCLUSION
In this work, we presented a workflow to generate 3D stochastic DFN models, with algorithm optimization for fracture plane clusterization. To obtain three-dimensional data, we interpreted a virtual outcrop model in an immersive environment. The main conclusions are listed as follows:

- The decision regarding the number of fracture sets, often disregarded, can be automatized by adapting the Elbow method to work with spherical data, reducing the user bias in the process;
- Clusterization data can be improved by the analysis of spherical statistics;

- The automatic cluster balancing brings more data quality for the stochastic processes generating fractures with similar behavior to the input data.

Additional future works aim to integrate the DFN model with multi-scale data from regional observations and porosity data to generate a representative geo-cellular model of the region. Also, further validation of the statistical models is to be carried out by incorporating machine learning techniques. Further analysis needs to be made concerning the number of interpretations to verify how representative to the DFN the acquired interpretations are. Concerning the proposed clustering method and definition of the number of clusters, future works will validate the proposed methods against other state-of-the-art clusterization methods.

CODE AVAILABILITY

The code script developed in Python and the related data is available at the Github repository (https://bit.ly/3vtOGRx), under the BSD-3 license.

CONTRIBUTORS

G.R. and A.M.J. conception and software development, analysis and interpretation of the data and drafting the article. G.R., A.M.J., and L.T. analyzed the results. G.R. and A.M.J. wrote the text. All authors reviewed the manuscript.

DECLARATION OF INTERESTS

The authors declare that they have no known competing financial interests or personal relationships that could have appeared to influence the work reported in this paper.

REFERENCES

[1] H. O. da Rocha, J. L. S. da Costa, A. A. G. Carrasquilla, and A. M. V. Carrasco, "Permeability estimation and analysis of fracture networks using resistivity logs in an offshore aptian carbonate reservoir pre-salt, in the southeastern Santos basin," *J. Appl. Geophys.*, vol. 184, Jan. 2021, Art. no. 104241.

[2] J. Lamarche, A. P. C. Lavenu, B. D. M. Gauthier, Y. Guglielmi, and O. Jayet, "Relationships between fracture patterns, geodynamics and mechanical stratigraphy in carbonates (South-east basin, France)," *Tectonophysics*, vol. 581, pp. 231–245, Dec. 2012.

[3] A. P. C. Lavenu and J. Lamarche, "What controls diffuse fractures in platform carbonates? Insights from provence (France) and apulia (Italy)," *J. Struct. Geol.*, vol. 108, pp. 94–107, Mar. 2018.

[4] K. Bjorlykke, *Petroleum Geoscience: From Sedimentary Environments to Rock Physics*, 2nd ed. Springer, 2010.

[5] D. C. P. Peacock, C. W. Nixon, A. Rotevatn, D. J. Sanderson, and L. F. Zuluaga, "Glossary of fault and other fracture networks," *J. Struct. Geol.*, vol. 92, pp. 12–29, Nov. 2016.

[6] Q. Lei, J.-P. Latham, and C.-F. Tsang, "The use of discrete fracture networks for modelling coupled geomechanical and hydrological behaviour of fractured rocks," *Comput. Geotechnics*, vol. 85, pp. 151–176, May 2017.

[7] A. Comerford, A. Fraser-Harris, G. Johnson, and C. I. McDermott, "Controls on geothermal heat recovery from a hot sedimentary aquifer in Guardbridge, Scotland: Field measurements, modelling and long term sustainability," *Geothermics*, vol. 76, pp. 125–140, Nov. 2018.

[8] A. Shahbazi, A. Saeidi, and R. Chesnaux, "A review of existing methods used to evaluate the hydraulic conductivity of a fractured rock mass," *Eng. Geol.*, vol. 265, Feb. 2020, Art. no. 105438.

[9] M. Pavlis and E. Cummins, "Assessing the vulnerability of groundwater to pollution in Ireland based on the COST-620 pan-European approach," *J. Environ. Manage.*, vol. 133, pp. 162–173, Jan. 2014.

[10] S. Bigi, M. Battaglia, A. Alemanni, S. Lombardi, A. Campana, E. Borisova, and M. Loizzo, "CO_2 flow through a fractured rock volume: Insights from field data, 3D fractures representation and fluid flow modeling," *Int. J. Greenhouse Control*, vol. 18, pp. 183–199, Oct. 2013.

[11] L. Guo, X. Li, Y. Zhou, and Y. Zhang, "Generation and verification of three-dimensional network of fractured rock masses stochastic discontinuities based on digitalization," *Environ. Earth Sci.*, vol. 73, no. 11, pp. 7075–7088, Jun. 2015.

[12] A. Giuffrida, F. Agosta, A. Rustichelli, E. Panza, V. La Bruna, M. Eriksson, S. Torrieri, and M. Giorgioni, "Fracture stratigraphy and DFN modelling of tight carbonates, the case study of the lower cretaceous carbonates exposed at the Monte alpi (basilicata, Italy)," *Mar. Petroleum Geol.*, vol. 112, Feb. 2020, Art. no. 104045.

[13] B. Lepillier, P.-O. Bruna, D. Bruhn, E. Bastesen, A. Daniilidis, Ó. Garcia, A. Torabi, and W. Wheeler, "From outcrop scanlines to discrete fracture networks, an integrative workflow," *J. Structural Geol.*, vol. 133, Apr. 2020, Art. no. 103992.

[14] M. Mauldon, W. M. Dunne, and M. B. Rohrbaugh, "Circular scanlines and circular windows: New tools for characterizing the geometry of fracture traces," *J. Struct. Geol.*, vol. 23, nos. 2–3, pp. 247–258, Feb. 2001.

[15] H. Watkins, C. E. Bond, D. Healy, and R. W. H. Butler, "Appraisal of fracture sampling methods and a new workflow to characterise heterogeneous fracture networks at outcrop," *J. Struct. Geol.*, vol. 72, pp. 67–82, Mar. 2015.

[16] S. William Dershowitz and H. Hans Herda, "Interpretation of fracture spacing and intensity," in *Proc. 33rd U.S. Symp. Rock Mech. (USRMS)*, 1992, pp. 757–766.

[17] T. Miyoshi, D. Elmo, and S. Rogers, "Influence of data analysis when exploiting DFN model representation in the application of rock mass classification systems," *J. Rock Mech. Geotech. Eng.*, vol. 10, no. 6, pp. 1046–1062, Dec. 2018.

[18] X. Wang, "Stereological interpretation of rock fracture traces on borehole walls and other cylindrical surfaces," Ph.D. dissertation, Fac. Virginia Polytech. Inst. State Unversity, Virginia Tech, 2005.

[19] S. D. Priest, *Discontinuity Analysis for Rock Engineering*. London, U.K.: Chapman & Hall, 1993.

[20] L. Jing and O. Stephansson, "The basics of fracture system characterization–field mapping and stochastic simulations," in *Developments in Geotechnical Engineering*, vol. 85. Amsterdam, The Netherlands: Elsevier, 2007, pp. 147–177.

[21] A. Giuffrida, V. La Bruna, P. Castelluccio, E. Panza, A. Rustichelli, E. Tondi, M. Giorgioni, and F. Agosta, "Fracture simulation parameters of fractured reservoirs: Analogy with outcropping carbonates of the inner apulian platform, Southern Italy," *J. Struct. Geol.*, vol. 123, pp. 18–41, Jun. 2019.

[22] L. Smeraglia, M. Mercuri, S. Tavani, A. Pignalosa, M. Kettermann, A. Billi, and E. Carminati, "3D discrete fracture network (DFN) models of damage zone fluid corridors within a reservoir-scale normal fault in carbonates: Multiscale approach using field data and UAV imagery," *Mar. Petroleum Geol.*, vol. 126, Apr. 2021, Art. no. 104902.

[23] N. Parrino, F. Agosta, P. Di Stefano, G. Napoli, F. Pepe, and P. Renda, "Fluid storage and migration properties of sheared neptunian dykes," *Mar. Petroleum Geol.*, vol. 102, pp. 521–534, Apr. 2019.

[24] D. Pan, S. Li, Z. Xu, Y. Zhang, P. Lin, and H. Li, "A deterministic-stochastic identification and modelling method of discrete fracture networks using laser scanning: Development and case study," *Eng. Geol.*, vol. 262, Nov. 2019, Art. no. 105310.

[25] W. Xu, Y. Zhang, X. Li, X. Wang, F. Ma, J. Zhao, and Y. Zhang, "Extraction and statistics of discontinuity orientation and trace length from typical fractured rock mass: A case study of the xinchang underground research laboratory site, China," *Eng. Geol.*, vol. 269, May 2020, Art. no. 105553.

[26] Y. Li, Q. Wang, J. Chen, L. Xu, and S. Song, "K-means algorithm based on particle swarm optimization for the identification of rock discontinuity sets," *Rock Mech. Rock Eng.*, vol. 48, no. 1, pp. 375–385, Jan. 2015.

[27] L. Gonzaga, M. R. Veronez, G. L. Kannenberg, D. N. Alves, L. G. Santana, J. L. de Fraga, L. C. Inocencio, L. V. de Souza, F. Marson, F. Bordin, F. M. W. Tognoli, K. Senger, and C. L. Cazarin, "A multioutcrop sharing and interpretation system: Exploring 3-D surface and subsurface data," *IEEE Geosci. Remote Sens. Mag.*, vol. 6, no. 2, pp. 8–16, Jun. 2018.

[28] P. Rossa, R. K. Horota, A. Marques Junior, A. S. Aires, E. M. De Souza, G. L. Kannenberg, J. L. De Fraga, L. Santana, D. N. Alves, J. Boesing, L. Gonzaga, M. R. Veronez, and C. L. Cazarin, "MOSIS: Immersive virtual field environments for earth sciences," in *Proc. IEEE Conf. Virtual Reality 3D User Interfaces (VR)*, Mar. 2019, pp. 1140–1141.

[29] O. L. Silva, F. H. R. Bezerra, R. P. Maia, and C. L. Cazarin, "Karst landforms revealed at various scales using LiDAR and UAV in semi-arid Brazil: Consideration on karstification processes and methodological constraints," *Geomorphology*, vol. 295, pp. 611–630, Oct. 2017.

[30] R. E. B. Araújo, V. La Bruna, A. Rustichelli, F. H. R. Bezerra, M. M. Xavier, P. Audra, J. A. Barbosa, and A. C. D. Antonino, "Structural and sedimentary discontinuities control the generation of Karst dissolution cavities in a carbonate sequence, Potiguar basin, Brazil," *Mar. Petroleum Geol.*, vol. 123, Jan. 2021, Art. no. 104753.

[31] R. K. Gomes, L. P. L. de Oliveira, L. Gonzaga, F. M. W. Tognoli, M. R. Veronez, and M. K. de Souza, "An algorithm for automatic detection and orientation estimation of planar structures in LiDAR-scanned outcrops," *Comput. Geosci.*, vol. 90, pp. 170–178, May 2016.

[32] Q. Feng, P. Sjögren, O. Stephansson, and L. Jing, "Measuring fracture orientation at exposed rock faces by using a non-reflector total station," *Eng. Geol.*, vol. 59, nos. 1–2, pp. 133–146, Jan. 2001.

[33] W. Richard Allmendinger, N. Cardozo, and M. D. Fisher, *Structural Geology Algorithms: Vectors and Tensors*. Cambridge, U.K.: Cambridge Univ. Press, 2011.

[34] I. Nicholas Fisher, T. Lewis, and J. J. Brian Embleton, *Statistical Analysis of Spherical Data*. Cambridge, U.K.: Cambridge Univ. Press, 1993.

[35] V. S. Cronin, "Finding the mean and 95 percent confidence interval of a set of strike-and-dip or lineation data," *Environ. Eng. Geosci.*, vol. 14, no. 2, pp. 113–119, May 2008.

[36] V. Kanti Mardia and E. Peter Jupp, "*Directional Statistics*, vol. 494. Hoboken, NJ, USA: Wiley, 2009.

[37] T. M. Kodinariya and P. R. Makwana, "Review on determining number of cluster in K-means clustering," *Int. J.*, vol. 1, no. 6, pp. 90–95, 2013.

[38] A. J. Riquelme, A. Abellán, and R. Tomás, "Discontinuity spacing analysis in rock masses using 3D point clouds," *Eng. Geol.*, vol. 195, pp. 185–195, Sep. 2015.

[39] D. Kong, C. Saroglou, F. Wu, P. Sha, and B. Li, "Development and application of UAV-SfM photogrammetry for quantitative characterization of rock mass discontinuities," *Int. J. Rock Mech. Mining Sci.*, vol. 141, May 2021, Art. no. 104729.

[40] A. Buyer and W. Schubert, "Calculation the spacing of discontinuities from 3D point clouds," *Proc. Eng.*, vol. 191, pp. 270–278, Jan. 2017.

[41] T. Möller and B. Trumbore, "Fast, minimum storage ray-triangle intersection," *J. Graph. Tools*, vol. 2, no. 1, pp. 21–28, 1997.

[42] O. C. da Pessoa Neto, U. M. Soares, J. G. F. da Silva, E. H. Roesner, C. P. Florencio, and C. A. V. de Souza, "Bacia potiguar," *Boletim de Geociências da PETROBRÁS*, vol. 15, no. 2, pp. 357–369, 2007.

[43] A. K. Alves de Medeiros and V. C. Córdoba, "Stratigraphic analysis of ponta do mel carbonate platform, albian-cenomanian in potiguar basin, NE of Brazil," *J. South Amer. Earth Sci.*, vol. 102, Oct. 2020, Art. no. 102675.

[44] J. A. G. Lopes, D. L. de Castro, and G. Bertotti, "Quantitative analysis of the tectonic subsidence in the Potiguar basin (NE Brazil)," *J. Geodyn.*, vol. 117, pp. 60–74, Jun. 2018.

[45] R. C. T. Cassab, "Paleontologia da Formação Jandaíra, Cretáceo Superior da Bacia Potiguar, comênfase na paleobiologia dos gastrópodos," Ph.D. thesis, Instituto de Geosciências, Univesidade Federal do Rio de Janeiro, Rio de Janeiro, Brazil, 2003, p. 184.

[46] S. D. Graaf, J. G. John Reijmer, H. R. Giovanni Bertotti, H. R. Francisco Bezerra, L. Caroline Cazarin, K. Bisdom, and B. Hubert Vonhof, "Fracturing and calcite cementation controlling fluid flow in the shallow-water carbonates of the Jandaíra Formation, Brazil," *Mar. Petroleum Geol.*, vol. 80, pp. 382–393, Feb. 2017.

[47] F. Daniel Menezes, H. Francisco Bezerra, F. Balsamo, A. Arcari, P. Rubson Maia, and L. Caroline Cazarin, "Subsidence rings and fracture pattern around dolines in carbonate platforms–Implications for evolution and petrophysical properties of collapse structures," *Mar. Petroleum Geol.*, vol. 113, Mar. 2020, Art. no. 104113.

[48] J. Robert Dunham, "Classification of carbonate rocks according to depositional textures," in *Proc. Classification Carbonate Rocks—A Symp.* (American Association of Petroleum Geologists), Tulsa, Oklahoma, 1962, pp. 108–121.

[49] G. Bertotti, S. D. Graaf, K. Bisdom, B. Oskam, B. Hubert Vonhof, H. R. Francisco Bezerra, J. G. John Reijmer, and L. Caroline Cazarin, "Fracturing and fluid-flow during post-rift subsidence in carbonates of the Jandaíra Formation, Potiguar Basin, NE Brazil," *Basin Res.*, vol. 29, no. 6, pp. 836–853, 2017.

[50] G. Juliana Rabelo, P. Rubson Maia, H. R. Francisco Bezerra, and C. Carlos Nascimento Silva, "Karstification and fluid flow in carbonate units controlled by propagation and linkage of mesoscale fractures, Jandaíra Formation, Brazil," *Geomorphology*, vol. 357, May 2020, Art. no. 107090.

[51] J. Matthew Westoby, J. Brasington, F. Niel Glasser, J. Michael Hambrey, and M. Jennifer Reynolds, "'Structure-from-motion' photogrammetry: A low-cost, effective tool for geoscience applications," *Geomorphology*, vol. 179, pp. 300–314, Dec. 2012.

[52] A. Corradetti, S. Tavani, M. Parente, A. Iannace, F. Vinci, C. Pirmez, S. Torrieri, M. Giorgioni, A. Pignalosa, and S. Mazzoli, "Distribution and arrest of vertical through-going joints in a seismic-scale carbonate platform exposure (Sorrento peninsula, Italy): Insights from integrating field survey and digital outcrop model," *J. Struct. Geol.*, vol. 108, pp. 121–136, Mar. 2018.

[53] Y. Furukawa and C. Hernández, "Multi-view stereo: A tutorial," *Found. Trends Comput. Graph. Vis.*, vol. 9, nos. 1–2, pp. 1–148, 2015.

[54] C. Duelis Viana, A. Endlein, G. Ademar da Cruz Campanha, and C. Henrique Grohmann, "Algorithms for extraction of structural attitudes from 3D outcrop models," *Comput. Geosci.*, vol. 90, pp. 112–122, May 2016.

[55] A. Esmaeilzadeh and K. Shahriar, "Shape effect of fractures on intensity and density of discreet fracture networks," *Periodica Polytechnica Civil Eng.*, vol. 63, no. 2, pp. 465–479, Apr. 2019.

[56] E. Panza, F. Agosta, A. Rustichelli, S. C. Vinciguerra, A. Ougier-Simonin, M. Dobbs, and G. Prosser, "Meso-to-microscale fracture porosity in tight limestones, results of an integrated field and laboratory study," *Mar. Petroleum Geol.*, vol. 103, pp. 581–595, May 2019.

[57] M. Usman, N. A. Siddiqui, S.-Q. Zhang, M. J. Mathew, Y.-X. Zhang, M. Jamil, X.-L. Liu, and N. Ahmed, "3D geo-cellular static virtual outcrop model and its implications for reservoir petro-physical characteristics and heterogeneities," *Petroleum Sci.*, vol. 18, no. 5, pp. 1357–1369, Oct. 2021.

[58] R. Battulwar, M. Zare-Naghadehi, E. Emami, and J. Sattarvand, "A state-of-the-art review of automated extraction of rock mass discontinuity characteristics using three-dimensional surface models," *J. Rock Mech. Geotech. Eng.*, vol. 13, no. 4, pp. 920–936, Aug. 2021.

[59] Y. Liang, F. He, and X. Zeng, "3D mesh simplification with feature preservation based on whale optimization algorithm and differential evolution," *Integr. Comput.-Aided Eng.*, vol. 27, no. 4, pp. 417–435, 2020.

[60] P. Gillespie, E. Monsen, L. Maerten, D. Hunt, J. Thurmond, and D. Tuck, "Fractures in carbonates: From digital outcrops to mechanical models," *Outcrops Revitalized*, vol. 11, pp. 137–147, Jan. 2011.

[61] G. Caravaca, S. Le Mouélic, N. Mangold, J. L'Haridon, L. Le Deit, and M. Massé, "3D digital outcrop model reconstruction of the kimberley outcrop (Gale crater, Mars) and its integration into virtual reality for simulated geological analysis," *Planet. Space Sci.*, vol. 182, Mar. 2020, Art. no. 104808.

GRACIELA RACOLTE graduated in cartographic and surveying engineering from Unisinos University, São Leopoldo, Brazil, in 2019. She received the master's degree in applied computing from Unisinos University, in 2021, where she is currently pursuing the Ph.D. degree. She is a also a Researcher at the Vizlab|X-Reality and Geoinformatics Laboratory, Unisinos University, working on the computer graphics and image processing research line.

ADEMIR MARQUES, JR., received the M.Sc. degree in computer science from São Paulo State University, Brazil, in 2016. He is currently pursuing the Ph.D. degree in applied computing with Unisinos University, São Leopoldo, Brazil. He is also a Researcher at the Vizlab|X-Reality and GeoInformatics Labortaory, Unisinos University, working on machine learning and pattern recognition for data analysis, image processing, and geo-statistics in geological data.

LEONARDO SCALCO received the bachelor's degree in civil engineering from Unisinos University, São Leopoldo, Brazil, in 2019, where he is currently pursuing the master's degree in applied computing. He is also a Researcher with the Vizlab|X-Reality and GeoInformatics Laboratory, Unisinos University, focusing on the study of roughness applied to fluid flow and geomechanics.

CAROLINE LESSIO CAZARIN received the M.Sc. degree from the Federal University of Rio de Janeiro, in 2015, and the Ph.D. degree in geology with focus in hypogenic karst from the University of Brasília, in 2021. He is currently a Geologist Specialist in karst processes and carbonate reservoirs at the Petrobras Research Center. Since 2013, he has been coordinating and managing of Research and Development Projects. His research interests include fractured and karstified reservoirs, flow simulation, and digital and virtual outcrop models.

LEANDRO TONIETTO received the M.Sc. and Ph.D. degrees in applied computing from Unisinos University, São Leopoldo, Brazil, in 2005 and 2021, respectively. He has held lecturing position at Unisinos University. His research interests include computer vision, image processing, real-time computer graphics, and graphics processing unit programming.

LUIZ GONZAGA, JR. (Member, IEEE) received the M.Sc. and Ph.D. degrees in electrical engineering from the State University of Campinas, Brazil, in 1996 and 2005, respectively. He was a Lecturer and a Professor at Unisinos University, São Leopoldo, Brazil, where he co-created and co-heads the Vizlab|X-Reality and GeoInformatics Laboratory. His research interests include computer vision, real-time computer graphics, graphics processing unit programming, and immersive visualization with a strong interest toward geoinformatics applications. He is currently a member of the IEEE Computer Society, the Association for Computing Machinery (ACM), the ACM Special Interest Group on Spatial Information, and the ACM Special Interest Group on Computer Graphics and Interactive Techniques.

DANIEL CAPELLA ZANOTTA received the M.Sc. degree in remote sensing from the Federal University at Rio Grande do Sul (UFRGS), Brazil, in 2010, and the Ph.D. degree in remote sensing from the National Institute for Space Research (INPE), São José dos Campos, Brazil, in 2014. He is currently a Postdoctoral Researcher at the Vizlab|X-Reality and Geoinformatics Laboratory, Unisinos University, Brazil.

MAURÍCIO ROBERTO VERONEZ received the M.Sc. and Ph.D. degrees in transportation engineering from the São Carlos School of Engineering, University of São Paulo, Brazil, in 1998 and 2004, respectively. He was a Lecturer and a Professor at Unisinos University, São Leopoldo, Brazil, where he co-created and co-heads the Vizlab|X-Reality and GeoInformatics Laboratory. His research interests include global navigation satellite systems, remote sensing, digital imaging, and immersive visualization with a strong bias on geoinformatics applications.

• • •